

Mingxuan ZHANG<sup>1,2</sup>, Hao ZHAN<sup>1,2</sup>, Baigang MI<sup>1,2</sup>, Yishan ZHANG<sup>1,2</sup>, Yan Liu<sup>1,2</sup>

<sup>1</sup>School of Aeronautics of Northwestern Polytechnical University, Xi 'an 710072, China

<sup>2</sup>National Key Laboratory of Aircraft Configuration Design, Xi'an, 710072, China

#### Abstract

Fragment warhead damage on aircraft exposes internal structure to the external flow field, altering aerodynamic characteristics and causing significant aerodynamic/structural coupling phenomena, which seriously threaten the aircraft's survivability. This study employs the AGARD455.6 standard model, on basis of considering fragment-damaged form characteristics, to construct fragment-damage wings by perforation and wing skin warping. Through computational structure dynamics (CSD) and computational fluid dynamics (CFD) two-way coupling time-domain simulation, this study analyzes the fragment-damage wing's flutter critical velocity and flutter characteristics at various Mach numbers and unveils the physical mechanism underlying the fragment-damaged influence on the flutter boundary. The results indicate that fragment-damaged wings flutter boundary always shifts forward, depending on the different degrees, locations, and forms of damage. As damage degree increases, the flutter boundary advances by up to 22.63%. Under a given damage degree, damage holes located in the wing's root result in more significant flutter boundary shift forward compared to those near the center or tip, with a maximum forward shift of 10.87%. For high-fidelity configurations with wing skin warping, at lower Mach numbers, the flutter boundary shifts backward by 6.34%. However, as the Mach number rises, the flutter boundary progressively shifts forward, achieving a maximum forward shift of 10.75%.

**Keywords:** fragments damage; wing; flutter critical velocity; CFD/CSD coupling; time-domain simulation

### 1. Introduction

With the rapid development of modern air defense weapons and the continuous improvement of flight mission requirements, the probability of typical fragment damage caused by air interception is also increasing <sup>[1]</sup>. When the major aerodynamic components are damaged, the aerodynamic characteristics and mass center will change, which causes significant flight state deviation and performance loss in short time, and the risk of crash will greatly rise <sup>[1]</sup>. Therefore, to improve aircraft survivability, it's necessary to pre-analyze the major aerodynamic components damage at the initial design to provide a reference for the aerodynamics margin design and flight control systems.







Fig 1 Aircraft main aerodynamic components damage since 20th century:(a) A380 airliner wing damage in 2003;(b) F16C fighter right wing damage in 2004;(c) A310 airliner rudder damage in 2005

The study of aircraft with typical fragment damage is deepening with war emerging. Many institutions and individuals domestic and foreign have carried out studies on damaged aircraft. In foreign research, NASA Ames Research Center, Langley Research Center, University of Virginia,

Rockwell Collins, MIT, Georgia Tech, Delft University of Technology and other universities and institutions have carried out different degrees of study[2]~[8]. NASA Ames Research Center and Langley Research Center derived the dynamic equation for asymmetric-structure GTM transport considering the changes in aerodynamic and dynamic characteristics. This study obtained a more accurate description of the damaged system. Ouellette studied the aerodynamic characteristics change on discrete damaged aircraft and used fitting method to obtain the aerodynamic parameters near the leveling point, Before 2010, Rockwell Collins completed the flight test of the sudden loss of 40%, 60% and 80% wing area on F-18 scale verification aircraft. Saeedi and Mani<sup>[9]</sup> from Amir Kabir University, based on the NACA641-412 airfoil, studied the circular damage, star damage and three repaired wing configurations. The results indicated that both circular damage and star damage can significantly reduce lift and produce drag, the degree of performance degradation depends on the fragment incident angle and jet coming out from damage hole. Mani and Render<sup>[10]</sup> conducted some experiments to determine the effects of triangular and star damage on the aerodynamic characteristics. Based on tunnel data, they proposed a technique to predict the effect of combat damage on wing's aerodynamic performance. Djellal[11] proposed two experimental studies to evaluate the performance degradation under weapon damage. The results indicated that significant aerodynamic performance degradation is related to the diameter, hole span-wise and hole chordwise. Etemadi<sup>[12]</sup> used experiments and CFD to evaluate the wing aerodynamic characteristics change under triangular damage and star damage. The results indicated that damage shape is important to damage wing performance evaluation and revealed the mechanism of structural damage influences aerodynamic force.

In domestic research, Mi B.G<sup>[13]</sup> constructed the flying-wing configurations with discrete and continuous damage. Based on the damaged configurations, this study established an identification method of coupled dynamic derivative and analyzed the dynamic aerodynamic coupling characteristics caused by geometric asymmetry. Chen Z. W <sup>[14]</sup> studied the influence of round hole damage on the wing aerodynamic characteristics. The results indicated that the position closer to the leading edge the more serious the lift loss of the wing. Cen Fei <sup>[15]</sup> used vortex lattice method to establish the aerodynamic calculation method of structural damage model. Zhang Feng <sup>[16]</sup> based on a certain fighter to establish the numerical simulation method on fragments and discrete damage, and compared the difference of longitudinal aerodynamic characteristics in cruise.

According to domestic and foreign research, because of the complexity of fragment damage, the present damage configurations are all smooth piercing or cutting surfaces, wing skin warping by actual killing is not taken into account. However, there is great difference between wing skin warping and smooth piercing, because when aircraft is damaged by fragments, the internal structure space will be exposed to flow field, which makes aerodynamic and structural mode coupling more obvious. Most of existing studies evaluate the aerodynamics characteristics change, the attention on aerodynamic/structural coupling is weak, that limits supporting significance of the study conclusions.

For the above problems, this paper constructs the high-fidelity fragment-damaged wing with skin warping and the simplified fragment-damaged wing with smooth perforation. Based on CFD/CSD two-way coupling time-domain simulation, establish the flutter boundary identification method for these constructions. Then further studies on the influence of damage diameter, damage quantity, damage position, and wing skin warping height on flutter boundary. It provides technical support for aircraft design, survivability evaluation and flight control fault-tolerant system design.

# 2. Typical Wing Damage Configurations Considering Wing Skin Warping Construction And Simplification

The actual aircraft combat damage structure is complex, the fragment damage in the battlefield will produce irregular geometric defects on wing structure, which will disturb aerodynamic and structural characteristics of the wing. The irregular defects are mainly reflected in two aspects: The one is when the fragment passes through the wing box, an internal space connected with the external space will form in the wing, which will change the local structural stiffness and form a complex cavity flow in the connected area. The other one is meanwhile fragment penetration occurs, because of the ductility of the metal wing skin, the penetrating process will cause serious deformation or even wing skin warping. When the wing skin warping reaches a certain height, the warped wing skin will further affect the flow distribution of the wing surface, and then change the aerodynamic force on the wing.

When constructing damage configuration, the main features should be retained, the cavity flow and wing skin warping caused by fragment damage are shown in Figure 2. Cavity and skin warping will cause local disturbance on the flow and structure of the wing, but the influence mechanism is not the same. The wing skin warping is always irregular and affected by the damaged position, material properties and so on. Therefore, these two damage characteristics should be retained.

This paper constructs two kinds of damage configurations, the one is the simplified model without wing skin warping, only considering fragment penetration. We use this configuration to explore the influence of different damage penetrations, damage locations and damage quantity on the flutter boundary, avoiding the uncertainty of skin warping equivalence under different damage positions and degrees. The other one is under certain damage conditions, constructing the high-fidelity configuration with wing skin warping, to explore the influence of different warping heights on flutter boundary.

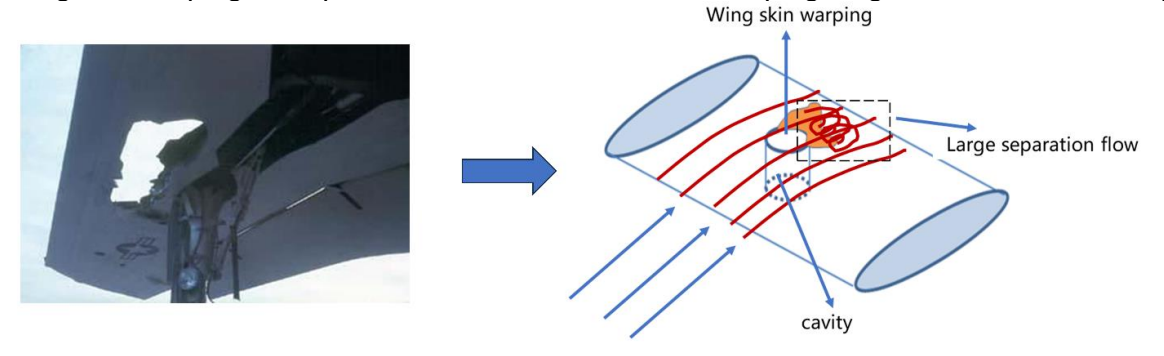


Fig 2 Aerodynamic disturbance mechanism of wing fragment damage

# 2.1 Wing Fragment Damage Simplified Configuration Construction

Because the damage location of the wing is relatively random, and the damage at different positions will bring different aerodynamic and structural disturbances. In this paper, we based on AGARD455.6 wing (standard example for flutter calculation) construct the simplified damage configuration. The simplified damage configuration is constructed by zonal design, mainly considering the flow distribution span-wise and chord-wise.

Figure 3-(a) shows the difference between the damage design location along span-wise and chord-wise. Simplified damage configurations do not consider the complex aerodynamic disturbance caused by skin warping, only used to study the influence of different damage degrees, locations and other factors on flutter boundary.

Figure 3-(b) ~ (f) covers all simplified damage configurations of ARAGD455.6. For the influence of damage hole size, this paper designs the damage holes with a hole diameter of 50mm, 70mm, 90mm at position 6 in Figure 3-(a), the configurations are shown in Figure 3-(a) (b) (c). For the influence damage holes quantity, opening damage holes are opened at positions 2,4,6 in Figure 3-(a) additionally, the configurations are shown in Figure 3-(d) (e) (f). For the influence of the damage holes span-wise position distribution, opening damage holes along the reference line at positions 2, 4 and 6 of Figure 3-(a), the configurations are shown in Figure 3-(c) (g) (h). For the influence of the damage holes chord-wise position distribution, opening damage holes along the reference line at positions 1 and 2 of Figure 3-(a), its geometric configuration is shown in Figure 3-(i) (j).

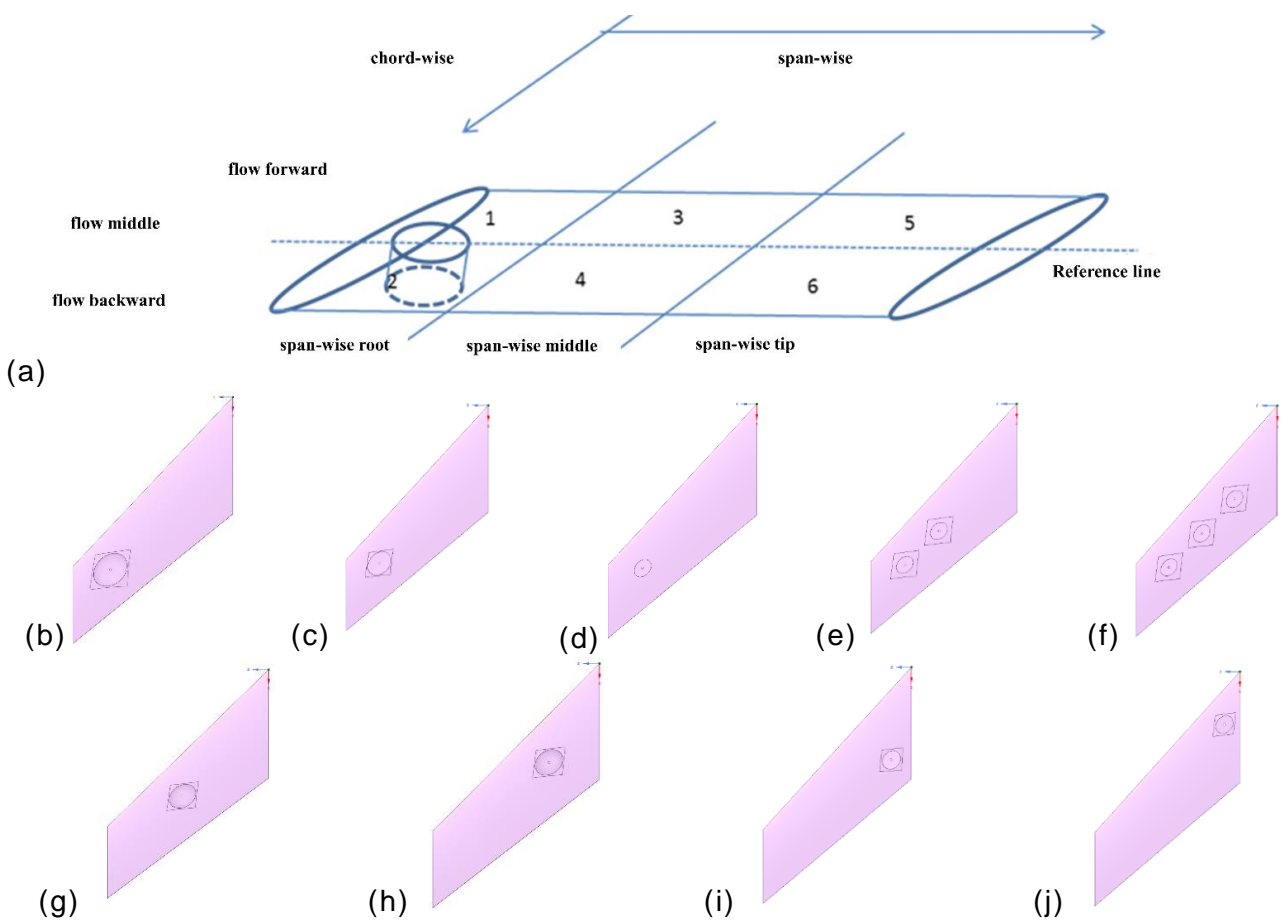
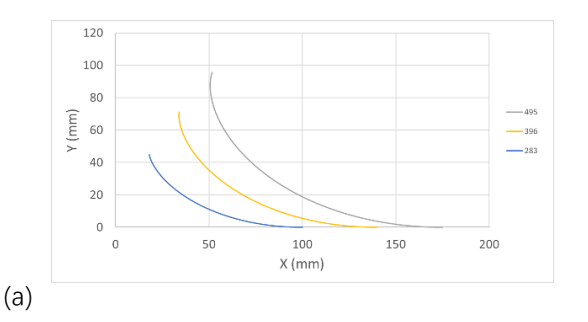


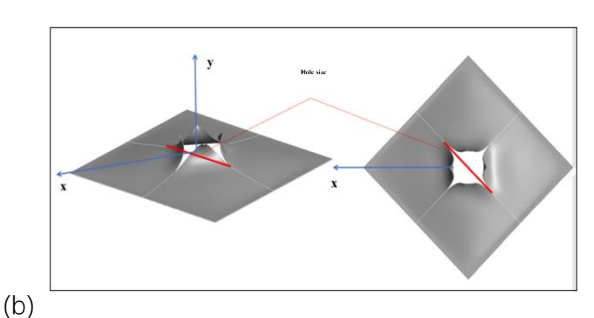
Fig 3 ARAGD455.6 all simplified configuration Design: (a) location distribution of damaged holes; (b) configuration 1 (single hole damage 90mm); (c) configuration 2 (single hole damage 70mm); (d) configuration 3 (single hole damage 50mm); (e) configuration 4 (double hole damage 50mm); (f) configuration 5 (three-hole damage 50mm); (g) configuration 6 (span-wise middle damage 70mm); (h) configuration 7 (span-wise root damage 70mm); (i) configuration 8 (chord-wise trailing edge damage 50mm); (j) configuration 9 (chord-wise leading edge damage 50mm)

# 2.2 High-Fidelity Wing Damage Configurations Construction

In this section we refer the experimental results of range<sup>[17][18]</sup>, and don't consider the area loss and extension by wing skin penetration determined damage location. On this premise, according to the area equivalent method, we construct typical fragment damage configurations of wings with different wing skin warping heights. The relationship between the wing skin and the warping area is shown in Figure 4-(a),(b). The damage was caused by a penetrating fragment on the wing's lower surface, and based on the water hammer effect<sup>[19][20]</sup>, forming an "exploding petal" warping on the upper surface.

Figure 4-(c)  $\sim$  (e) covers all high-fidelity damage configuration design of ARAGD455.6. According to different damage degrees, the wing skin warping height will be different. At position 6 of Figure 3-(a), based on aperture 30mm, 40mm, 50mm to construct the wing skin warping damage holes with heights of 6.4mm, 10.1mm and 13.7mm, the configurations are shown in Figure 4-(c)  $\sim$  (e).





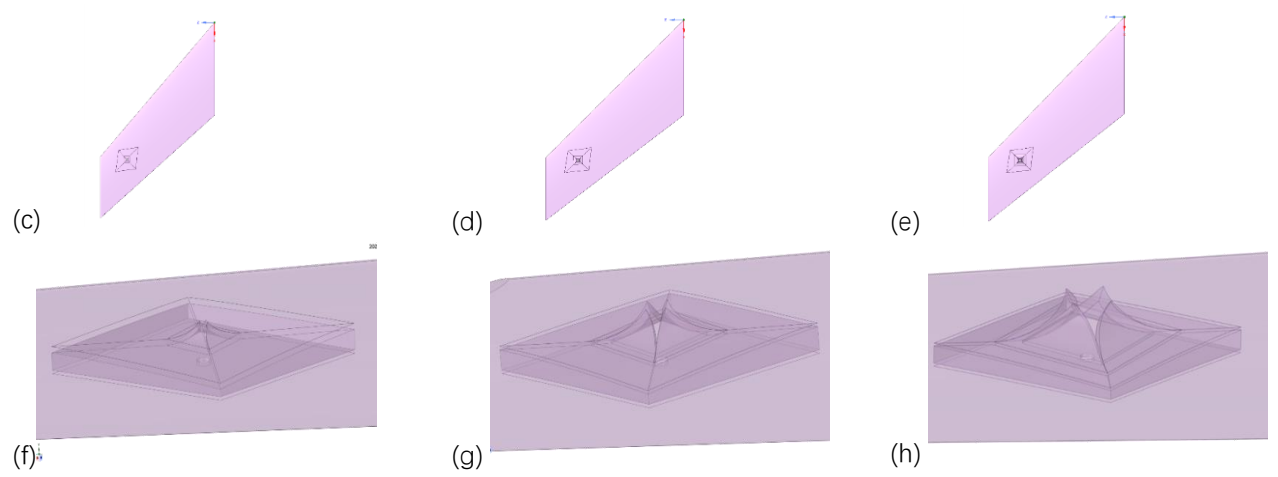


Figure 4 High-fidelity damaged wing configuration design: (a)wing skin warping design curve; (b)wing skin warping equivalent area; (c) configuration 10 (6.4mm wing skin warping damage); (d) configuration 11 (10.1mm wing skin warping damage); (e) configuration 12 (13.7mm wing skin warping damage); (f) 6.4mm wing skin warping local details; (g) 10.1mm wing skin warping local details; (h) 13.7mm wing skin warping local details;

# 3. Fragment Damage Configuration Flutter Characteristics Based On Cfd/Csd Coupling Time-Domain Simulation

# 3.1 CFD/CSD TWO-WAY COUPLING NUMERICAL CALCULATION METHOD

Flutter can be evaluated in frequency-domain or time-domain<sup>[21]</sup>, the calculation cost of the frequency domain method is low and the flutter critical velocity can be calculated quickly. However, the damage configurations have non-linear local flow field due to perforation and skin warping, so the common frequency domain model is not applicable. Therefore, this paper analyzes flutter critical velocity through a time-domain CFD/CSD two-way coupling method.

For CFD calculation, the governing equations are based on continuity equation, momentum equation and energy equation. The three-dimensional compressible N-S equations are as follows: continuity equation

$$\frac{\partial \rho}{\partial t} + \frac{\partial \left(\rho u_{j}\right)}{\partial x_{i}} = 0 \tag{1}$$

momentum equation

$$\frac{\partial(\rho u_i)}{\partial t} + \frac{\partial}{\partial x_i} (\rho u_i u_j) = -\frac{\partial p}{\partial x_i} + \frac{\partial \tau_{ij}}{\partial x_i}$$
(2)

energy equation

$$\frac{\partial(\rho E)}{\partial t} + \frac{\partial}{\partial x_{j}} (\rho E u_{j}) =$$

$$-\frac{\partial}{\partial x_{i}} (p u_{j}) - \frac{\partial q_{j}}{\partial x_{i}} + \frac{\partial}{\partial x_{i}} (u_{i} \tau_{ij})$$
(3)

In the above formula,  $\rho$  is the density of the fluid, uj is the velocity component of the fluid in the direction j, p is the pressure, E is the total energy. This paper solves numerical solution by Reynolds Average Navier-Stokes (RANS) equation and k-w SST turbulence model.

For numerical calculation of wing flutter, we need to consider wing deformation under aerodynamic force and calculate its structural model. The solid will deform and move under the aerodynamic force, the governing equation is as follows:

$$M_{c}\ddot{u} + C_{c}\dot{u} + K_{c}u = F \tag{4}$$

In the above formula, Ms is mass matrix, Cs is damping matrix, Ks is stiffness matrix, F is aerodynamic force,  $\ddot{u}$ ,  $\ddot{u}$ , u are nodes acceleration, velocity and displacement. Newmark implicit time integration method is used for numerical solution.

To verify the accuracy of the numerical calculation, we use AGARD 455.6 wing and base on

Ansys-Workbench, using Fluent and Mechanical to realize CFD&CSD two-way coupling numerical simulation method, the basic process is shown in Figure 5.

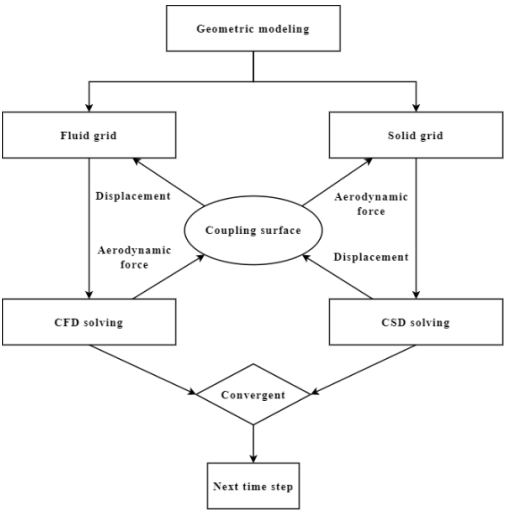


Figure 5 CFD&CSD two-way coupling flow

In the process of the time-domain analysis method, for the coupling interface between fluid and solid, the displacement and stress will conservative, so the governing equation is as follows:

$$n \cdot \tau_f = n \cdot \tau_s$$

$$r_f = r_s \tag{5}$$

In the above formula,  $\tau$ ,  $\gamma$  are the stress and displacement at the fluid-solid coupling surface; n is normal unit vector at the coupling surface; f represents fluid and f represents solid. For the data transfer on the coupling interface, this paper uses the feature preservation method.

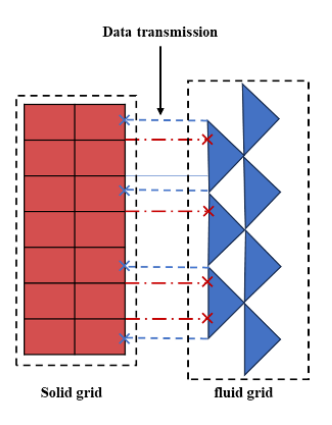


Figure 6 Coupling surface feature preservation method

# 3.2 Example Verification

In this paper, we use AGARD445.6 standard model to verify the time-domain analysis method. The model aspect ratio is 1.6525, the root-shoot ratio is 0.6576, backward angle is 45° at 1/4 wing chord.

Table 1. AGARD 445.6 material property table

Young's r	modulus (109	Pa)	Poisson's	s ratio		Shear mo	dulus (10 <sup>8</sup> Pa)	
X	Y	Z	XY	YZ	XZ	XY	YZ	XZ
3.23	0.42	0.42	0.31	0.31	0.31	4.093	4.392	4.392

The material properties are set up concerning the transonic wind tunnel flutter experiment of

NASA Langley Research Center<sup>[22]</sup>, as shown in Table 1. The calculated angle of attack is 0°, Mach number is based on the existing experiments, taking 0, 0.678, 0.901, 0.499, the fluid and solid computing grid is shown in Figure 7. The main modal patterns by simulation are shown in Figure 8. The comparative errors between the simulation modal characteristics and the experimental values are shown in Table 2. The results show that the maximum error is less than 3.3%. The main mode accords with the law of "one-bend, two-torsion, three-bend and four-torsion". Further, identify the flutter critical velocity by the time domain simulation method, results are shown in Table 3. Compared with the experimental values at different Mach numbers, the maximum error of flutter critical velocity is 7.4%, which shows that this method is relatively reliable.

Table 2. AGARD 445.6 Frequency comparison table of the first four modes

Mode order	Exp/Hz	CSD/Hz	Error	
First	9.5992	9.2808	3.317%	
Second	38.166	38.014	0.398%	
Third	48.3482	47.853	1.024%	
Forth	91.5448	91.753	0.227%	

Table 3. AGARD 455.6 flutter critical velocity comparison of this paper and Exp

	Ma=0.499	Ma=0.678	Ma=0.901	Ma=0.96
Vc-Exp	0.4459	0.4174	0.3700	0.3076
Vc-CFD/CSD	0.4557	0.4193	0.3604	0.2846
coupling				
Error	2.2%	0.46%	2.6%	7.4%

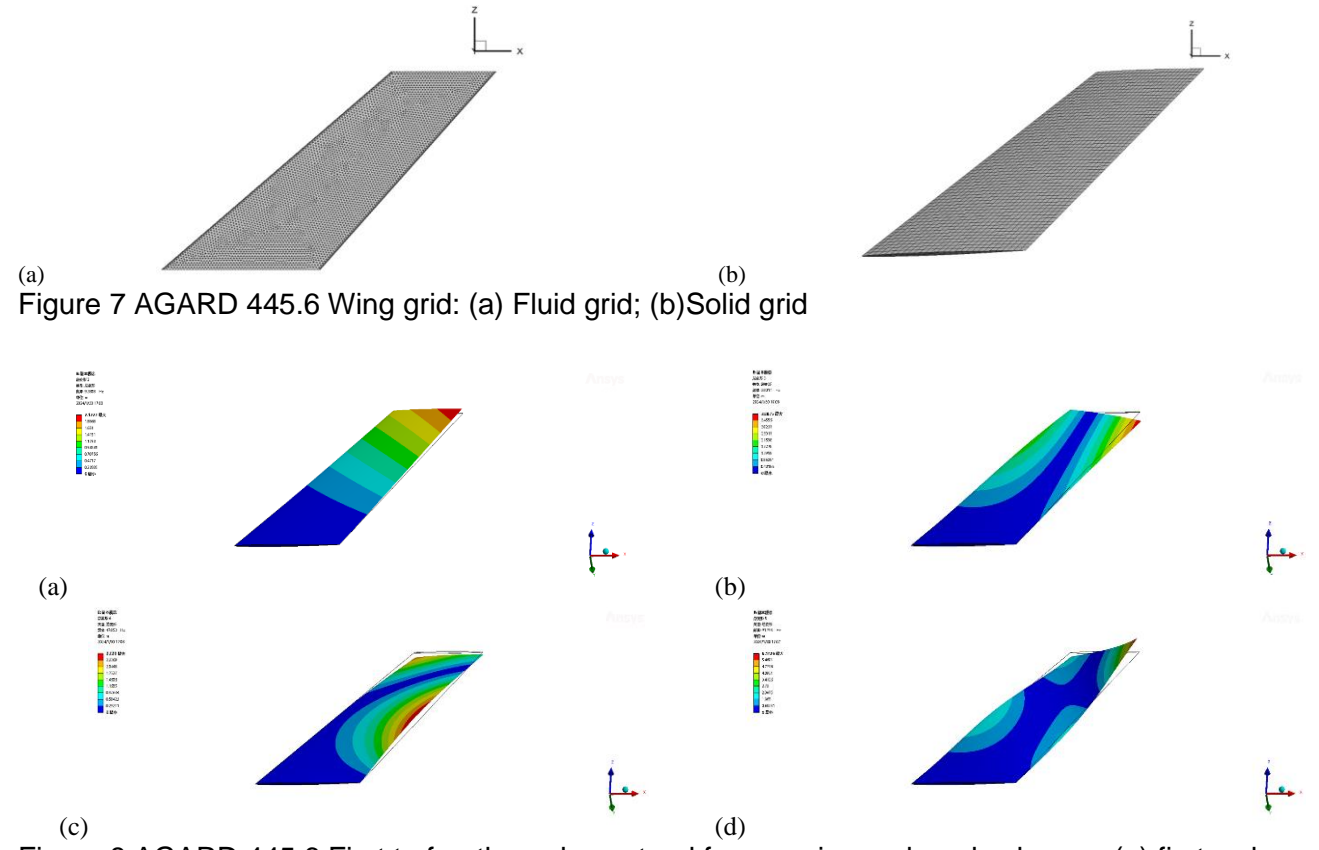


Figure 8 AGARD 445.6 First to fourth modes natural frequencies and mode shapes: (a) first-order mode (f=9.2808); (b) second-order mode (f=38.014); (c) third-order mode (f=47.853); (d) forth-order mode (f=91.753)

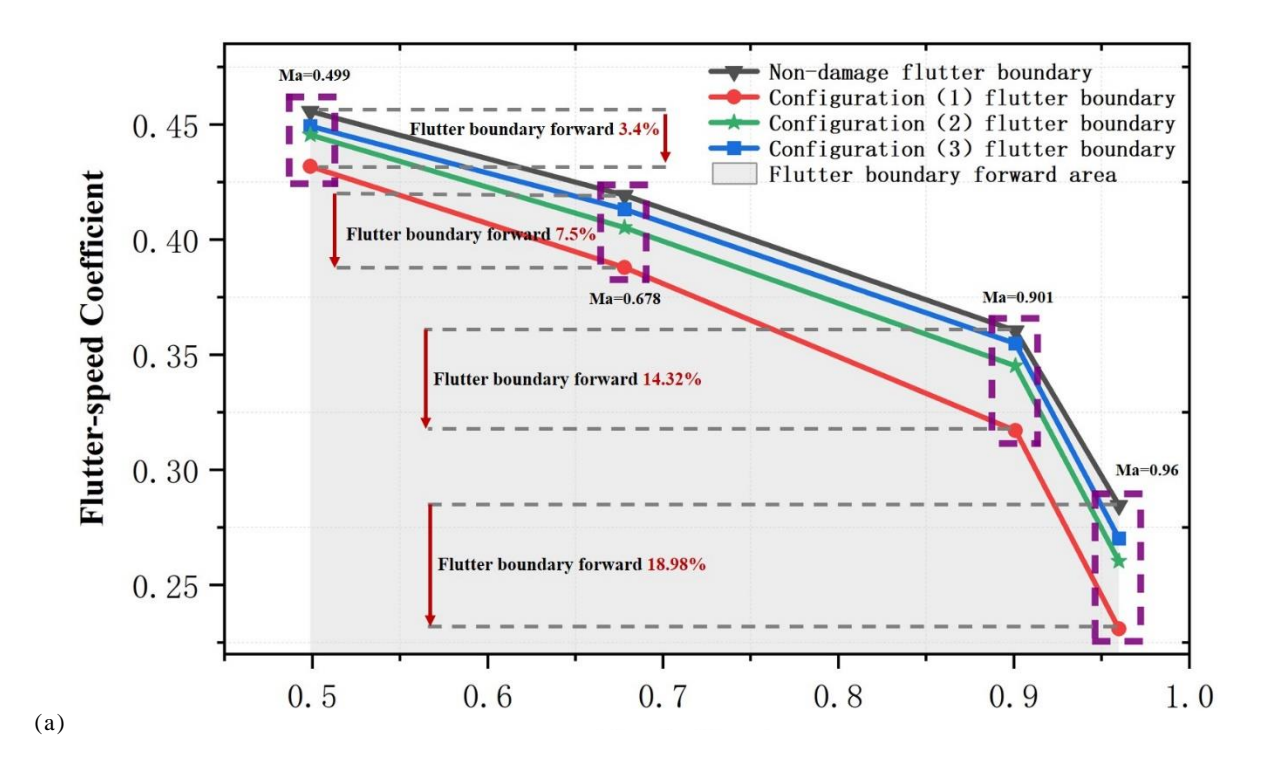
# 4. Flutter Characteristics Analysis Of Damage Configuration

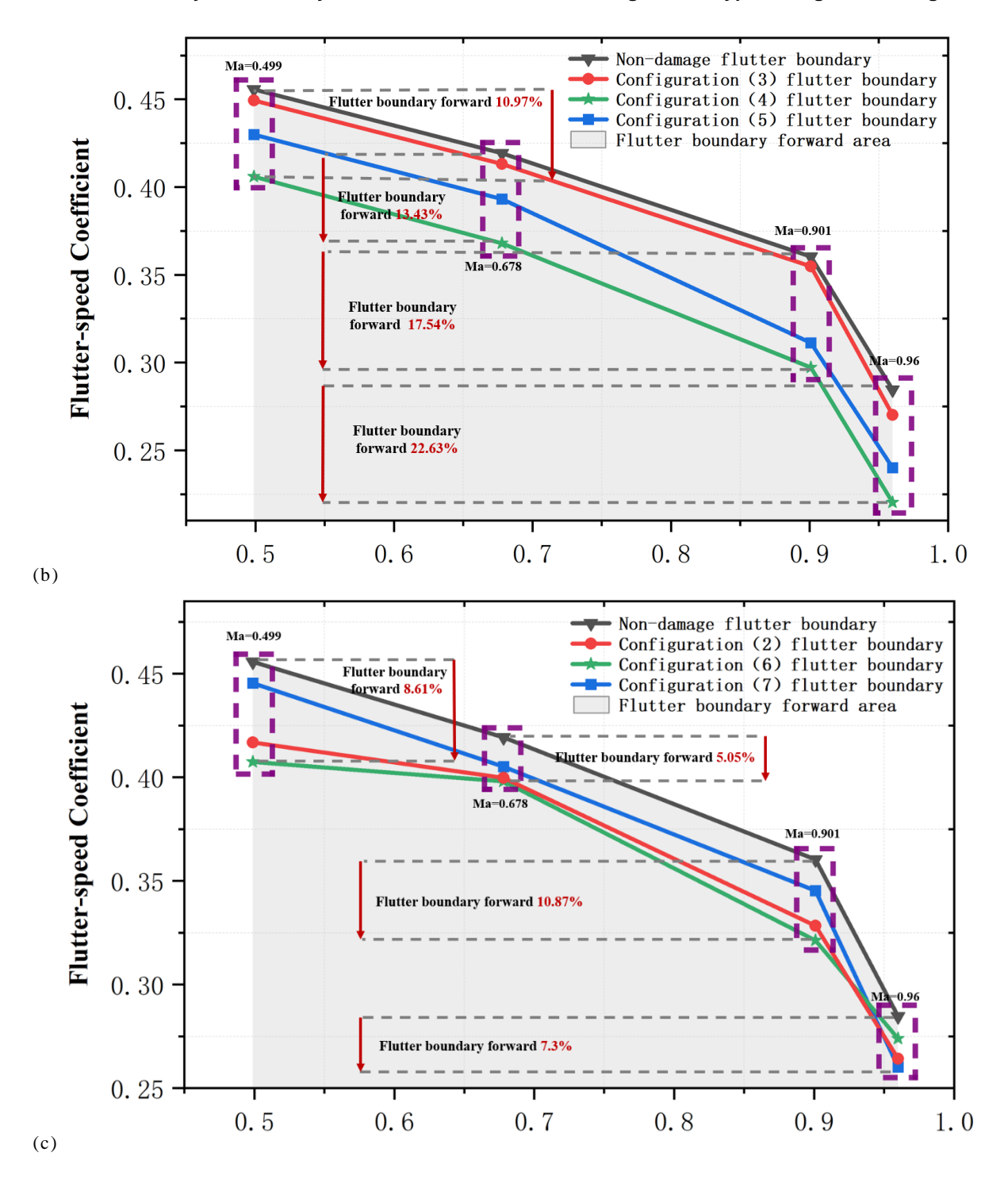
## 4.1 The Influence Of Damage Form On Flutter Boundary

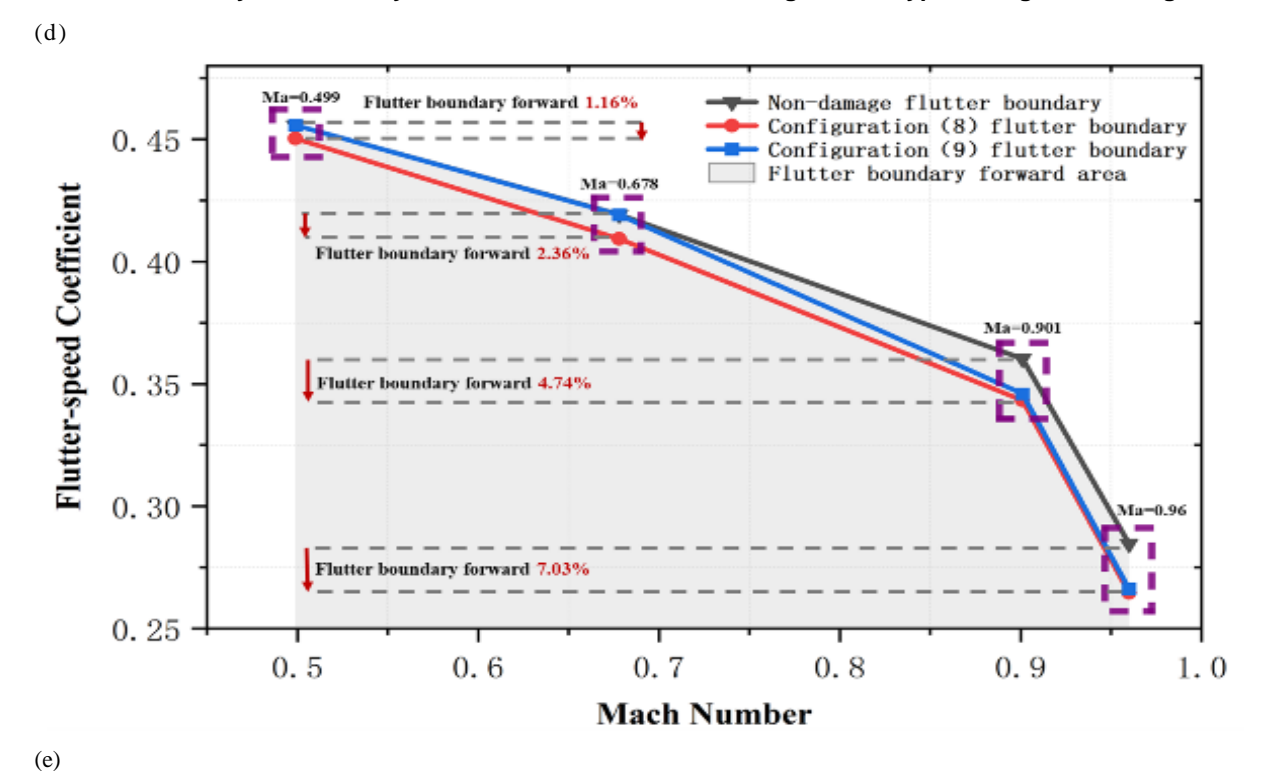
This part bases the numerical method in section 3.2, faces the simplified configuration of wing

fragment damage (configuration 1 ~ configuration 9) and wing skin warping high-fidelity configuration of (configuration 10 ~ configuration 12), calculates the flutter boundary at Mach number 0.499, 0.678, 0.901, 0.96. The results are shown in Figure 9 (a) ~ (f), comparing flutter boundaries of different damage configurations can indicate as follows:

- 1) The light gray area in the figure is divided by the non-damage configuration flutter boundary. Its physical significance is that in this area, the flutter boundary points are moved forward compared with the non-damage configuration, meaning the flutter occurs simply. In Figure 9 (a) ~ (e), 53 states (94.6%) flutter boundary moved forward, and only 3 states (5.4%) flutter boundary moved backward. From the overall trend, the flutter boundary of the wing moves forward after the wing is damaged.
- 2) From Figure 9 (a), (b), (e), with the increase of the degree of damage, the forward shift of flutter boundary increases. From Figure 9 (c), the closer damaged hole is to wing root, the forward shift of the flutter boundary increases. From Figure 9 (d), as the damaged hole moves to the trailing edge of the wing, the forward shift of the flutter boundary is increased.
- 3) The maximum forward shift of the flutter boundary under different Mach numbers is shown in Figure 9 (a)  $\sim$  (e). It can be seen that the larger Mach number, the greater forward shift of the flutter boundary, and the excitation effect of damage on the flutter is more obvious.







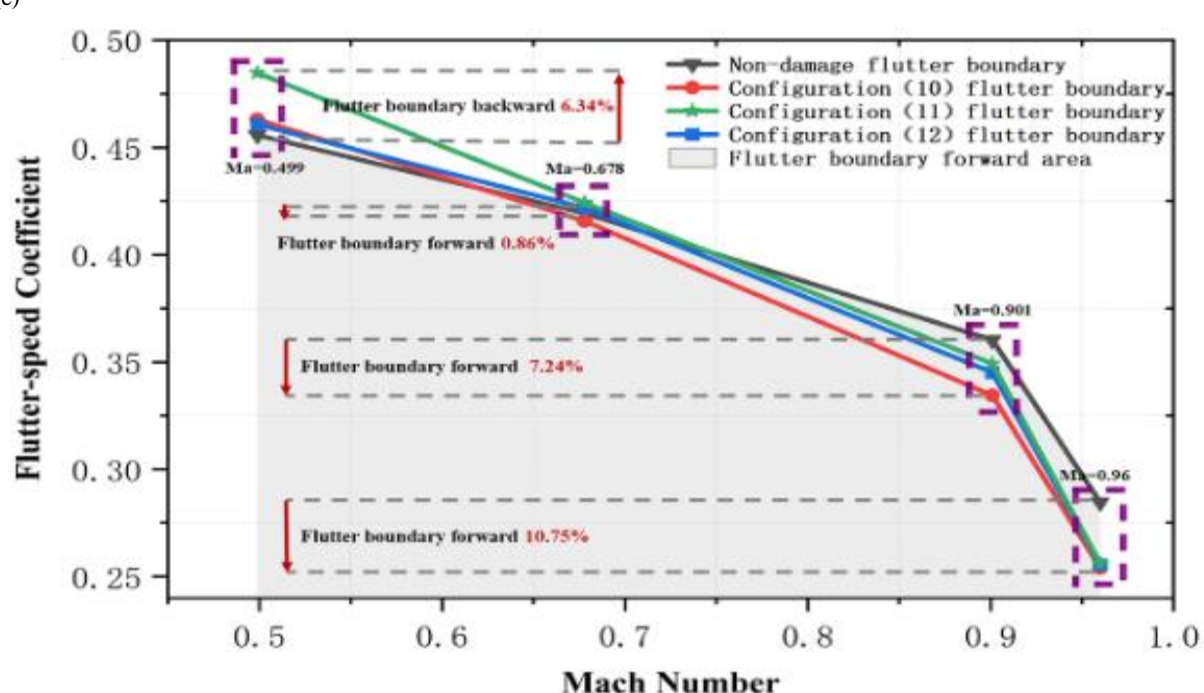


Figure 9 ARAGD455.6 Wing flutter critical Velocity under different damage forms: (a) different damage aperture size; (b) different damaged holes quantity; (c) different damaged hole spanwise distribution; (d) different damaged hole chord-wise distribution; (e) high-fidelity damage configuration

# 4.2 Influence Mechanism Of Damage Characteristics On Flutter Boundary

The classical flutter mechanism of AGARD455.6 wing is as follows. With the action of unsteady aerodynamic force, the frequencies of the wing's two unstable modes "bend and torsion" will get closer as the speed increases. Then reach the coupling state within a certain range, realize the process of mutual excitation between the aerodynamic force and structure, and finally excite the flutter.

This section discussed the influence mechanism of damage on flutter, according to the influence of different damage forms on aerodynamic characteristics and structural modal characteristics. For aerodynamic force, we use fast Fourier transform to extract the damaged wing's main frequency

changes at different dimensionless velocities. For the structural mode, we used the modal decomposition method to obtain the modal frequency change under different damage degree.

Table 4 shows the second-order torsion frequency disturbance of the different damage configurations with the change of damage degree. It can be seen from the table that the greater the degree of damage is, the more wing structure modal characteristics change drastically.

The copyright statement is included in the template and must appear in your final pdf document in the position, style and font size shown below. If you do not include this in your paper, ICAS is not allowed and will not publish it.

Table 4. Wing second-order torsion mode change trend under different damage forms

configuration	second-order mode/Hz	error
Non-damage	38.014	0.398%
Configuration2	36.775	3.259%
Configuration4	35.615	6.311%
Configuration5	34.472	9.318%
Configuration6	36.589	3.749%
Configuration7	36.675	3.522%
Configuration10	37.361	1.718%
Configuration11	37.131	2.323%
Configuration12	37.045	2.549%

Selecting eight damage configurations with different damage degrees, locations and wing skin warping heights, extract the aerodynamic dominant frequency under Mach number 0.499,0.678,0.901,0.96, as shown in Figure 11 (a) ~ (d). The non-damage configuration dominant frequency boundary represents the flutter excited boundary frequency. Combining the dominant frequency variation of the unsteady aerodynamic force in Figure 11 with the modal frequency change of the structure in Table 4, we can draw the following conclusions:

- 1) With the continuous increase of Mach number, more and more damage configuration dominant frequency points are higher than the non-damage configuration dominant frequency. After the damage, the dominant frequency of the aerodynamic force is increasing, and the modal frequencies of all the damaged structures show a downward trend, it makes the aerodynamic excitation frequency of the damaged configuration closer to the structure modal frequency with the increase of velocity. Therefore, flutter is simpler to be excited after damage, and this phenomenon reflected in section 4.1 is the trend of flutter boundary moving forward as a whole.
- 2) With the increase of Mach number, the damaged porous form aerodynamic dominant frequency firstly beyond a large range than non-damage configuration. Then, with the further increase of Mach number, the span-wise distribution of damage and damage with wing skin warping cross the non-damage boundary.

Combined with Table 4, porous damage configuration structure modal frequency decreases the most. This shows that with the increase of damage degree, it has both the fastest response to the increase of aerodynamic excitation frequency and the most severe influence on the structure modal frequency. Therefore, when the degree of damage is increasing, it will be simpler to excite the flutter. The phenomenon reflected in section 4.1 is that the flutter boundary moves forward earliest with the increase of the number of damaged holes, and with the Mach number increases, the forward shift amplitude.

3) The high-fidelity wing skin warping damage configuration has little effect on the structure modal frequency. Due to the existence of warping, the flow produces a more obvious separation at the damaged hole, this makes the flow more unstable and the frequency of energy concentration is higher at high Mach numbers. Figure 10 shows the flow field of the high-fidelity configuration as speed increases. The phenomenon reflected in section 4.1 is when the Mach number reaches 0.901 and 0.96, the high-fidelity configuration flutter boundary moves forward obviously. When the Mach

number is small(in this paper, Ma=0.499,0.678), the aerodynamic dominant frequency decreases compared with the non-damage configuration, and the flutter boundary tends to move backward.

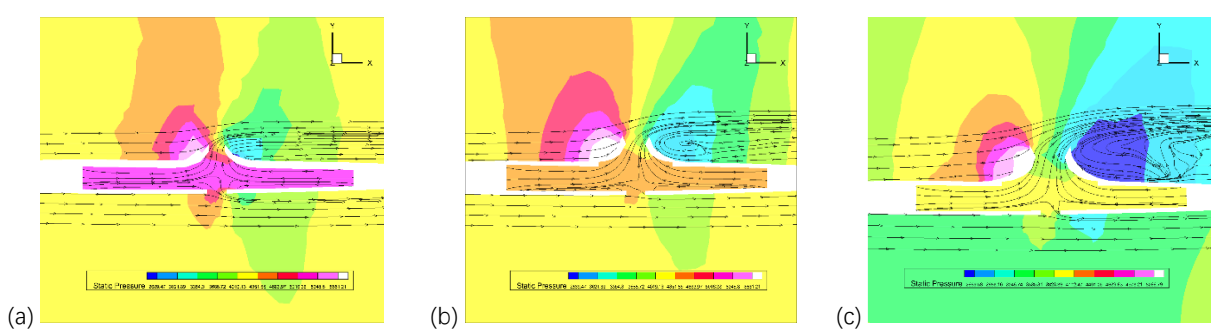
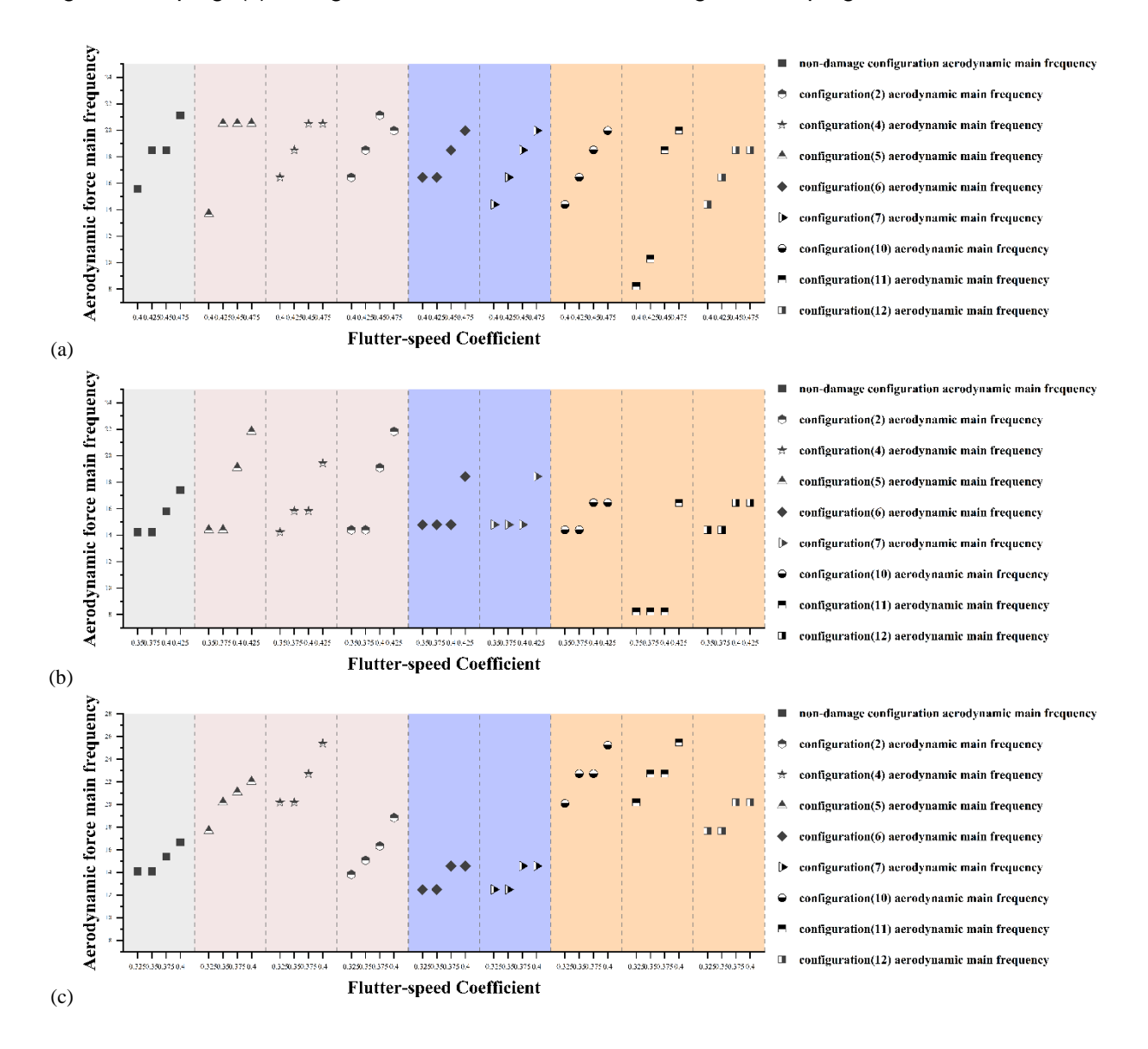


Figure 10 Flow chart of high-fidelity configuration and simplified configuration at the hole: (a) configuration 10 flow field slice at wing skin warping; (b) configuration 11 flow field slice at wing skin warping; (c) configuration 12 flow field slice at wing skin warping



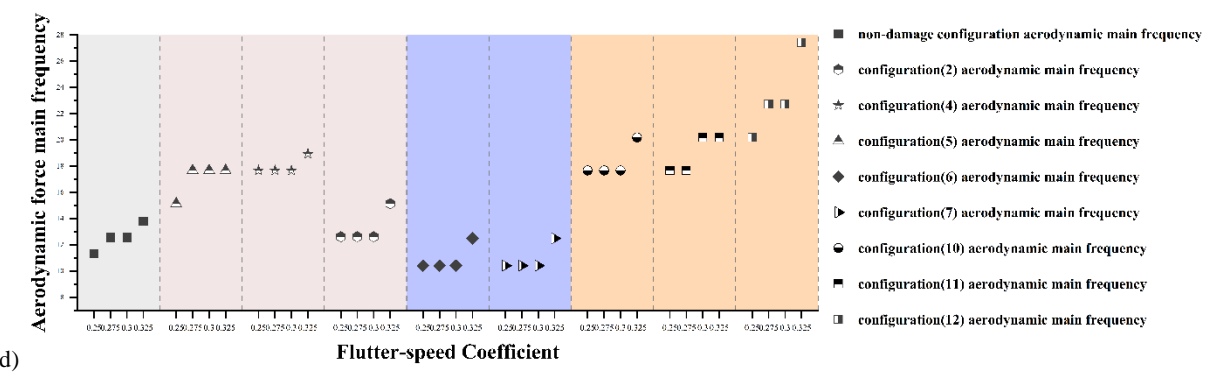


Figure 11 ARAGD 455.6 Unsteady aerodynamic main frequency distribution of different damage forms of wings under different Mach numbers: (a) Ma= 0.499; (b) Ma=0.678; (c) Ma=0.901; (d) Ma=0.96

#### 5. Conclusions

In this paper, we based on the AGARD455.6 standard model construct simplified analysis configuration and high-fidelity analysis configuration by considering wing skin warping or not, totally of 5 categories and 12 forms. Calculating different damage forms flutter boundaries under different Mach numbers, analyzing the movement regular of flutter boundary. Based on the influence of damage forms on the structural mode and the unsteady aerodynamic dominant frequency, we analyze the mechanism of flutter boundary movement. The main conclusions of the effects of different damage forms on the flutter boundary are as follows:

- 1) As the degree of damage increases, the elevation of the aerodynamic dominant frequency is simpler to excite at a lower Mach number, at the same time, the reduction of the structure modal frequency is more significant. So, the greater the damage degree is, the simpler wing flutter boundary moves forward, and with the increase of Mach number, the maximum forward movement can reach 22.63%.
- 2) For damage to different positions, the damage hole of the wing center increases aerodynamic main frequency more obviously with the increase of Mach number, and the reduction of the structural modal frequency of the wing root, the center and the tip is low. Therefore, as the damage holes are distributed to the root of the wing, the flutter boundary of the wing is simpler to move forward. However, due to the limited degree of damage, the maximum forward displacement can be up to 10.87%.
- 3) For high-fidelity damage with wing skin warping, only when the Mach number reaches a certain value (in this paper Ma =0.901), the wing skin warping can obviously reflect the increase of aerodynamic main frequency. Before this, wing skin warping showed a decreasing trend towards aerodynamic main frequency, and under the same damage degree, different wing skin warping heights have little effect on the reduction of structural modal frequency. So, compared to simplifying the damage configuration, at the same degree and location of damage, the existence of warping will cause the flutter boundary backward when the Mach number is low (in this paper Ma =0.499 and 0.678), the maximum backward displacement can reach 6.34%. When the Mach number increases to a certain extent (in this paper Ma =0.901 and 0.96), the flutter boundary will move forward obviously, with the increase of Mach number, the maximum forward movement of the flutter boundary can reach 10.75%.

## 6. Contact Author Email Address

Mingxuan ZHANG: zhangmingxuan@mail.nwpu.edu.cn.

#### 7. Acknowledgement

The authors would like to acknowledge the support of National Natural Science Foundation of China (Grant No. 12202363) and the support of Key Laboratory Fund (Grant No.D5150240005).

## 8. Copyright Statement

The authors confirm that they, and/or their company or organization, hold copyright on all of the original material included in this paper. The authors also confirm that they have obtained permission, from the copyright holder of any third party material included in this paper, to publish it as part of their paper. The authors confirm that they give permission, or have obtained permission from the copyright holder of this paper, for the publication and distribution of this paper as part of the ICAS proceedings or as individual off-prints from the proceedings.

#### 9. Reference

- [1] Wang GJ, 2021. "Research on anti-damage and fault-tolerant control system of UAV." Master's Thesis. Dalian University of Technology, Dalian, China.
- [2] Kim K, Ahn JM, Kim SK, Kim DM, et al., 2013. "Flight test of a flying-wing type UAV with partial wing loss using neural network controller." AIAA guidance, navigation, and control (GNC) conference, p. 5169.
- [3] Almond MT, Render P and Walker AD., 2015. "Analysis of single hole simulated battle damage on a wing using particle image velocimetry." In 33rd AIAA Applied Aerodynamics Conference, p. 2573.
- [4] Jourdan D, Piedmonte M, et al., 2010, August. "Enhancing UAV survivability through damage tolerant control." In AIAA Guidance, Navigation, and Control Conference, p. 7548.
- [5] Baur S, Annaswamy A, Gibson T, et al., 2011. "Simulation and adaptive control of a high agility model airplane in the presence of severe structural damage and failures." In AIAA guidance, navigation, and control conference, p. 6412.
- [6] Chowdhary G, Johnson E, Kimbrell MS, et al., 2010. "Flight test results of adaptive controllers in presence of severe structural damage." In AIAA Guidance, Navigation, and Control Conference, p. 8010.
- [7] Kim B.M, Sung D.Y, Sung J.M. and Kim B.S., 2009. "Integrated guidance and control design based on adaptive neural network for unpowered air vehicle." Journal of Institute of Control, Robotics and Systems, 15(1):15-22.
- [8] Saeedi M, Ajalli F and Mani M., 2010. "A comprehensive numerical study of battle damage and repairs upon the aerodynamic characteristics of an aerofoil." the aeronautical journal, 114(1158): 469-484.
- [9] Ouellette J A, 2010. "Flight dynamics and maneuver loads on a commer-cial aircraft with discrete source damage." Master's Thesis, Virginia Polytechnic Institute and State University, Blacksburg, USA.
- [10] Mani M and Render P., 2005. "Experimental investigation into the aerodynamic characteristics of airfoils with triangular and star shaped through damage." In 23rd AIAA Applied Aerodynamics Conference, p. 4978.
- [11] Djellal S, Ouibrahim A and Render PM., 2006. "The Influence of Battle Damage on the Aerodynamic Characteristics of a Model of an Aircraft." WSEAS Transactions on Fluid Mechanics, 1(1):89.
- [12] Etemadi F, Etemadi M, Mani M and Pooladsanj S., 2017. "Experimental and numerical analysis of aerodynamic effects of repair patches on damaged airfoils." Journal of Mechanical Science and Technology, 31:651-658.
- [13] Mi BG, 2021. "Simulation on the dynamic stability derivatives of battle-structure-damaged aircrafts." Defence Technology, 17(3):987-1001.
- [14] Chen ZW, 2018. "Research on Aerodynamic Simulation and Performance Degradation Analysis Method of Damaged Aircraft." Master's Thesis, Northwestern Polytechnical University, Xi'an, China.
- [15] Cen F, Li Q, et al., 2019. "The invention relates to an aerodynamic optimization calculation method for aircraft structural damage." CN Patent 109697329A.
- [16] Zhang F, Han Q and Liu X., 2013. "Study on Longitudinal Aerodynamic Performance of Fighting Damaged Aircraft." Aeronautical Computing Technique, 43(2): 48-50+55.
- [17] Xu ZX, Liu Y, et al., 2020. "Experimental Investigation on the Damage of Aircraft Subjected to Different Fragments Loading." Acta Armamentari, 41(S2): 63-68.
- [18] Dong QY, 2013. "Study on the damage of wing skin under the action of fragments and shock waves." Master's Thesis, Nanjing University of Aeronautics and Astronautics, Nanjing, China.
- [19] Zhang JF, Jia HB, et al., 2023. "Damage of hydrodynamic ram effect to riveted fuel tanks." Explosion and Impact, 43(07):123-135.
- [20] Han L, Han Q and Yang S., 2018. "Simulation analysis of hydrodynamic ram in an arcraft fuel tank subjected to high-velocity multi-fragment impact." Explosion and Shock Waves, 38(03):473-484.
- [21] Ye ZY, Zhang WW, Shi AM, et al., 2010. "Fundamentals of fluid-structure coupling and its application, 2nd Edition." Harbin Institute of Technology Press, Harbin, China, p.53-234.
- [22] Yates EC, 1988, July. "AGARD standard aeroelastic configurations for dynamic response, I-wing 445.6. AGARD." NASA Langley Research Center, USA.